arXiv:2403.10383v1 [math.DS] 15 Mar 2024

SCATTERING BETWEEN A VORTEX DIPOLE AND A POINT VORTEX: INSIGHTS FROM A NEW PHASE PLANE

ATUL ANURAG, ROY H. GOODMAN, ELLISON O'GRADY

Abstract. We study the scattering of a vortex dipole by a point vortex in the Helmholtz model of point-vortex interactions. We reduce a system of three vortices by stages to a one-degree-of-freedom conservative system. We relate properties of the scattering dynamics to features in the phase space of the reduced system. We first change variables to the Jacobi coordinates, followed by a Nambu reduction. This shows that the natural phase space of this problem is the upper sheet of a two-sheeted hyperboloid, which degenerates to an upper half-cone in a critical case. Gröbli (1877) derived the standard reduction of this system in which the system's state is represented by the lengths of the triangle's sides. The new coordinate system overcomes two related shortcomings of Gröbli's reduction that have made understanding the dynamics difficult: the lack of a phase plane and the singularity at all configurations in which the vortices are collinear. We then generalize the problem to consider when the circulation of the third, initially stationary, vortex differs from the circulations of the two that form the propagating dipole.

1. Introduction

The mutually-induced motion of point vortices in a two-dimensional inviscid incompressible fluid is a classical topic in fluid mechanics. The positions of the vortices are described by a Hamiltonian system of ordinary differential equations that has been well-studied over 150 years [23, 26]. These ODEs remain relevant because of their deep connection to turbulence in Bose-Einstein condensates and other quantum fluids, as summarized, for example, in Ref. [22].

In this paper, we develop a phase-plane approach to the scattering of three such vortices. It is well-known that two vortices with circulations of identical magnitude but opposite orientation form a *dipole* that propagates at constant velocity perpendicular to the line joining them. The presence of a third vortex can deflect its uniform motion, an example of *scattering*. Three such scattering solutions are shown in Fig. 1.1, in which the third vortex has the same absolute circulation as the two that form the dipole. While these three solutions obey very similar conditions as $t \to -\infty$, their behavior as $t \to \infty$ are quite different. Subfigures (a) and (b) show *exchange scattering* events: the dipole that exits the collision region is not composed of the same two vortices as the dipole that entered. By contrast, subfigure (c) displays *direct scattering*; the same two vortices form the dipole before and after the interaction. In addition to tracking whether the scattering event is of exchange or direct type, a usual question is to find a formula for the angle between the direction of propagation of the entering and exiting dipoles. These two questions have already been answered in separate papers by Aref and Lydon et al. in [2, 22]. Here, we derive a new reduced form of the equations of motion that sheds significant light on the scattering process. Since the dynamics of larger point vortex systems largely consist of a sequence of isolated three-vortex interactions, this should be useful in other vortex dynamics problems.

First, we discuss the need for a new reduction of three-vortex dynamics. Phase-space visualization and analysis are among the most important tools in dynamical systems, but the most commonly used form of the three-vortex equations makes phase-space reasoning difficult. Consider, by analogy, the pendulum. By the nineteenth century, the equations of motion for the well-known to be

Date: March 18, 2024.

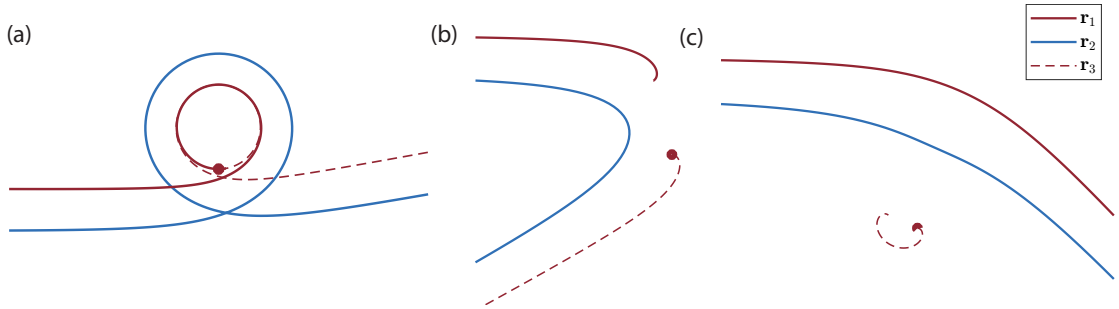

FIGURE 1.1. Three solutions of the scattering problem showing (a) Exchange scattering for $\rho = -0.999$. (b) Exchange scattering for $\rho = 2.5$. (c) Direct Scattering for $\rho = 3.8$. The vortex dipole arrives from $-\infty$ traveling parallel to the x axis, and vortex 3 sits at rest at the marked point as $t \to -\infty$.

integrable, and the exact solution could be found in terms of the Jacobi elliptic integrals $\mathrm{sn}\,(\phi, k)$, $\mathrm{cn}\,(\phi, k)$, and $\mathrm{dn}\,(\phi, k)$, and its period in terms of the complete elliptic integral $K(k)$. Today, such solutions are rarely taught and are needed only to obtain specific quantities, such as the period of an orbit. Instead, we teach students about the pendulum's phase space, which is most naturally represented as a cylinder whose coordinates are given by the pendulum's angle and angular velocity; see Fig. 1.2. The earliest publication we can find of the pendulum phase space is in the 1937 book of Andronov and Chaikin [1]. An educated reader can easily pick out all the features of the dynamics from this image: it has two fixed points, a center corresponding to the stable downward-pointing equilibrium and a saddle corresponding to the unstable inverted equilibrium. The center is surrounded by a family of closed curves corresponding to the librations. The limit of this family is a pair of homoclinic orbits connecting the inverted equilibrium to itself, and on the other side of the homoclinic orbits, closed curves encircling the cylinder corresponding to rotational periodic orbits. This diagram helps us reason about the dynamics: since both the librating and rotating families of periodic orbits limit to the homoclinic orbit, we may conclude there exist initial conditions arbitrarily close to each other, on opposite sides of the homoclinic orbit, with very different dynamics. Because orbits slow down as they approach a fixed point, the orbits' periods diverge as they approach the homoclinic orbit.

The equations of motion for a system of point vortices were first derived by Helmholtz and put into Hamiltonian form by Kirchhoff [19, 33]. Gröbli's 1877 doctoral thesis was the first detailed exploration of their solutions. In it, he derived the most commonly used reduction of the three-vortex system, a closed system of equations for the side lengths ℓ_j of the triangle with vertices at the three vortices. This system and others derived from it are used in most subsequent studies of the three-vortex problem [2, 6, 24, 27, 30, 31]. Aref and his collaborators researched this history extensively [5, 23]. We have translated the dissertation into English [12].

This reduction, however, is ill-suited to phase-space reasoning, though past researchers have made some progess [2, 30]. The coordinates ℓ_j must satisfy the triangle inequality, so not all triples (ℓ_1, ℓ_2, ℓ_3) represent physical configurations that satisfy this constraint. Let $\mathcal{D}_{\text{phys}} \subset \mathbb{R}^3$ denote the domain of physical configurations. Each point on its interior represents two triangles that are mirror images. The boundary $\partial\mathcal{D}_{\text{phys}}$ consists of collinear configurations of the three vortices. Such arrangements are common: many families of periodic orbits pass through such states twice per period, and three of the five possible rigidly rotating configurations of three vortices are collinear. Since the equations are singular on $\partial\mathcal{D}_{\text{phys}}$, linearization fails, and even finding the linear stability of the collinear states is difficult. More advanced reasoning, such as separating orbits into different families, like the librating and rotating pendulum orbits, is similarly difficult. The singularity of the

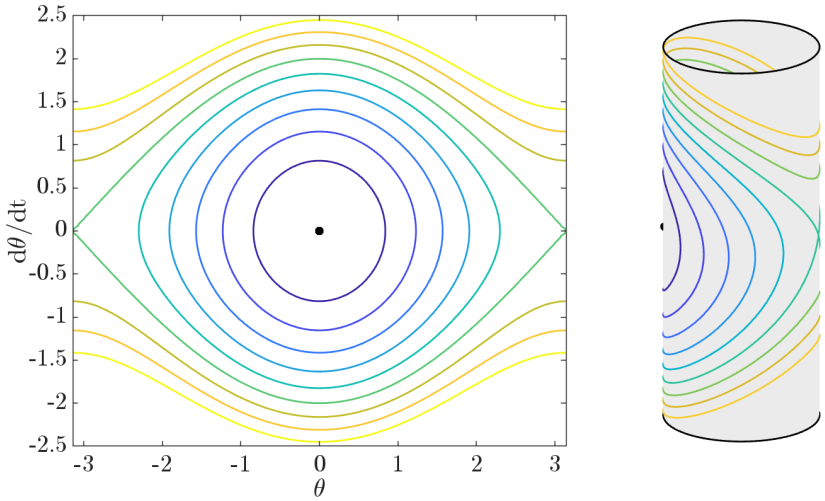

FIGURE 1.2. The phase space of the pendulum, in the plane and wrapped into a cylinder; after [1].

reduced ODE system is an artifact of the reduced coordinate system. It is not present in the vortex motion equations, which are only singular at configurations where two or more vortices occupy the same location. An alternate system of equations, based on the *angles* between the sides of the triangle and the radius of its circumcircle, has proved useful in certain situations but suffers from similar artificial singularities[3, 20].

The chief innovations of this paper are introducing a new reduction of the equations of motion that makes phase-space reasoning significantly easier and using this phase-plane to obtain a more thorough understanding of the scattering.

The paper is organized as follows. In Sec. 2, we introduce the equations of motion of the N-vortex system and review the Hamiltonian formalism used to study them. In Sec. 2.1, we focus on the problem of three vortices with circulations $\Gamma_1 = \Gamma_2 = -\Gamma_3 = 1$ and set up the scattering problem of interest. Sec. 3 reduces the system to the form needed to analyze the dynamics and is divided into subsections. We use Jacobi coordinates to reduce the number of degrees of freedom from three to two in Sec. 3.1 and then introduce Nambu brackets to further reduce the system in Sec. 3.2. In Sec. 3.3, we pause to interpret the relationship between the fully reduced coordinate system and the laboratory frame, allowing us to understand the new coordinates geometrically. Sec. 3.4 discusses how to recover two angles important for describing the dynamics: the system's orientation and the heading of the third vortex. This last quantity, when integrated, gives the scattering angle. Sec. 4 contains our analysis and visualization of the reduced system: we discuss its fixed points and singularities in Sec. 4.1 and visualize and interpret its phase space in Sec. 4.2. The separatrices divide the phase space into regions of topologically equivalent trajectories by the separatrices, and these, in turn, allow us to identify important transitions in the dynamics in Sec. 4.3. In Sec. 5, we generalize to the case where the initially stationary vortex has circulation $\Gamma \neq 1$, generalizing the reduction in Sec. 5.1, the phase space visualization in Sec. 5.2 and the explanation of the scattering in Sec. 5.3. We conclude in Sec. 6 with a discussion of the possible future applications of the coordinate reduction method.

2. The N-vortex system

The point-vortex model idealizes a near-two-dimensional inviscid incompressible fluid in which the vorticity is confined to a finite number of discrete points that induce a velocity that, in turn, causes the vortices to move. It is a standard topic in elementary fluid mechanics textbooks such as [9] and is well covered in Newton's textbook devoted to the subject [26].

Helmholtz derived the model of point-vortex motion describing the interaction of N point vortices, defined by the system of $2N$ ODEs in 1858 [33]:[1]

$$\frac{\mathrm{d}x_i}{\mathrm{d}t} = -\sum_{j\neq i}^{N} \Gamma_j \frac{(y_i - y_j)}{\|\mathbf{r}_i - \mathbf{r}_j\|^2}, \quad \frac{\mathrm{d}y_i}{\mathrm{d}t} = \sum_{j\neq i}^{N} \Gamma_j \frac{(x_i - x_j)}{\|\mathbf{r}_i - \mathbf{r}_j\|^2}. \tag{2.1}$$

Here $\mathbf{r}_i = \langle x_i, y_i \rangle$ denotes the position of the ith point vortex and Γ_i represents its circulation. The equations conserve an energy

$$H(\mathbf{r}_1, \ldots, \mathbf{r}_N) = -\frac{1}{2} \sum_{i<j}^{N} \Gamma_i \Gamma_j \log \|\mathbf{r}_i - \mathbf{r}_j\|^2. \tag{2.2}$$

In 1876, Kirchhoff noted that system (2.1) has a Hamiltonian formulation [19],

$$\frac{\mathrm{d}x_i}{\mathrm{d}t} = \frac{1}{\Gamma_i} \frac{\partial H}{\partial y_i}, \quad \frac{\mathrm{d}y_i}{\mathrm{d}t} = -\frac{1}{\Gamma_i} \frac{\partial H}{\partial x_i}. \tag{2.3}$$

This system possesses a Poisson bracket

$$\{F(\mathbf{r}), G(\mathbf{r})\} = \sum_{i=1}^{N} \frac{1}{\Gamma_i} \left(\frac{\partial F}{\partial x_i} \frac{\partial G}{\partial y_i} - \frac{\partial F}{\partial y_i} \frac{\partial G}{\partial x_i} \right). \tag{2.4}$$

Together with the chain rule, this implies that any function $F(\mathbf{r})$ evolves according to

$$\frac{\mathrm{d}F}{\mathrm{d}t} = \{F, H\}. \tag{2.5}$$

The factor of $\frac{1}{\Gamma_i}$ in these equations means that Hamiltonian system (2.3) is not quite in canonical form. This may be remedied by introducing variables

$$q_i = \sqrt{|\Gamma_i|} x_i \quad \text{and} \quad p_i = \sqrt{|\Gamma_i|}\, \mathrm{sign}(\Gamma_i) y_i, \tag{2.6}$$

which renders both the equations and the Poisson brackets into the canonical forms

$$\frac{\mathrm{d}q_i}{\mathrm{d}t} = \frac{\partial H}{\partial p_i}, \quad \frac{\mathrm{d}p_i}{\mathrm{d}t} = -\frac{\partial H}{\partial q_i}. \tag{2.7}$$

and

$$\{F, G\} = \sum_{i=1}^{N} \left(\frac{\partial F}{\partial q_i} \frac{\partial G}{\partial p_i} - \frac{\partial F}{\partial p_i} \frac{\partial G}{\partial q_i} \right). \tag{2.8}$$

Using these coordinates generally renders the equations harder to read and interpret so that we will avoid them except at one crucial step of the following reduction.

System (2.1) has three well-known conservation laws, which we write as

$$\mathbf{M} = \langle M_x, M_y \rangle = \sum_{i=1}^{N} \Gamma_i \mathbf{r}_i, \quad \text{and} \quad \Theta = \sum_{i=1}^{N} \Gamma_i \|\mathbf{r}_i\|^2. \tag{2.9}$$

[1] We systematically ignore a factor of $\frac{1}{2\pi}$ on the right-hand side of these equations and all that follows. This amounts to a rescaling of time.

The quantities $\mathbf{M}$ and Θ are called the *linear impulse* and the *moment of vorticity*, respectively. In the case that $\Gamma_{\text{tot}} = \sum_{i=1}^{N} \Gamma_i \neq 0$, then

$$\mathbf{r}_0 = \mathbf{M}/\Gamma_{\text{tot}} \tag{2.10}$$

defines the location of the conserved center of vorticity.

2.1. **The three-vortex system and dipole-vortex scattering.** We consider a system of three vortices: the vortices at positions $\mathbf{r}_1$ and $\mathbf{r}_2$ having circulation $+1$ and the vortex at $\mathbf{r}_3$ with circulation -1, previously considered in several other works [2, 22]. It is the subject of sections 3-5 of Gröbli's dissertation [5, 14].

This system has Hamiltonian

$$H = -\frac{1}{2}\log\|\mathbf{r}_1 - \mathbf{r}_2\|^2 + \frac{1}{2}\log\|\mathbf{r}_1 - \mathbf{r}_3\|^2 + \frac{1}{2}\log\|\mathbf{r}_2 - \mathbf{r}_3\|^2. \tag{2.11}$$

The conserved center of vorticity is thus

$$\mathbf{r}_0 = \mathbf{r}_1 + \mathbf{r}_2 - \mathbf{r}_3 \tag{2.12}$$

and the angular impulse is

$$\Theta = \|\mathbf{r}_1\|^2 + \|\mathbf{r}_2\|^2 - \|\mathbf{r}_3\|^2. \tag{2.13}$$

The Hamiltonian for the N-vortex system (2.1) with $N = 1$ vanishes identically. Therefore, a single point vortex remains in its initial position for all time. When $N = 2$ and the two vortices have equal strength and opposite circulation, they form a *dipole* that moves with constant velocity along the perpendicular bisector to the segment connecting them. Several previous studies have examined the behavior of the three-vortex system in which a dipole impinges on a stationary vortex. A schematic of this setup is shown in Fig. 2.1. A dipole consisting of a positive-circulation vortex at position $\mathbf{r}_1 = \langle -L, \rho + \frac{d}{2}\rangle$, where $L \gg 1$, and a negative-circulation vortex at position $\mathbf{r}_3 = \langle -L, \rho - \frac{d}{2}\rangle$ propagates to the right toward a positive-circulation vortex at position $\mathbf{r}_2 = \langle 0, -d\rangle$. These are chosen to set $\mathbf{r}_0 = 0$. Without loss of generality, we take $d = 1$. This is justified given the invariance of system (2.1) under rescaling of space and time, as discussed by Chapman [8].

Eventually, vortex 3 escapes to infinity as part of a dipole. We call the case when the escaping dipole comprises vortices 1 and 3 a *direct* scattering event and the case when it comprises vortices 2 and 3 an *exchange* scattering event.

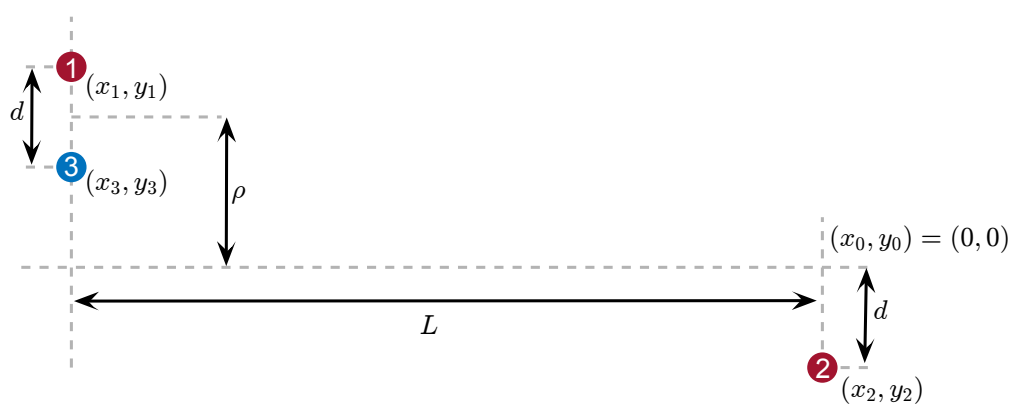

FIGURE 2.1. Setup of the scattering problem. The dipole formed by vortices 1 and 3 propagates toward the target, vortex 2. Without loss of generality, we take $d = 1$ throughout the study.

Examples are shown in Fig. 1.1. The initial conditions are posed as in the schematic, showing exchange scattering in panels (a) and (b) and direct scattering in panel (c). Since vortex 3 has opposite circulation to the two others, it must be part of both the entering and exiting dipoles. We define the *scattering angle* $\Delta\alpha$ to be its change of heading; see Eq. (3.26). Figure 2.2 shows the scattering angle as a function of the offset ρ, with the scattering angles of the three solutions shown in Fig. 1.1 marked.

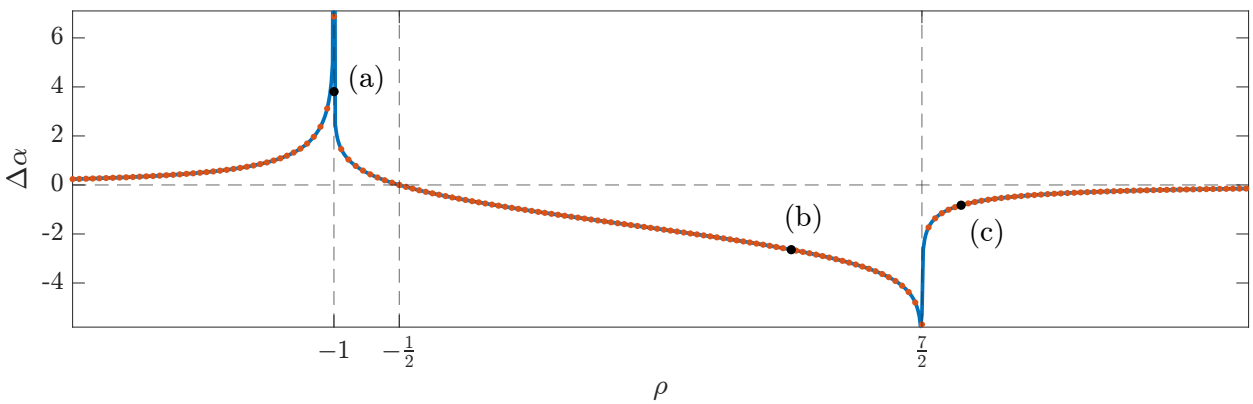

FIGURE 2.2. The deflection of the angle of vortex 3 plotted as a function as the distance ρ, showing singularities at $\rho = -1$ and $\rho = \frac{7}{2}$ as expected. The solid line is the result of direct simulation, and the red dots are the formulas derived in Appendix A. The points marked (a)–(c) correspond to the three simulations shown in Fig. 1.1.

If $|\rho| \gg 1$, the isolated vortex will scarcely deflect the dipole, so direct scattering will occur. Previous authors have determined, via fairly involved calculations, that exchange scattering occurs for $-1 < \rho < \frac{7}{2}$ [2, 22], and direct scattering outside this interval. The points $\rho = -1$ and $\rho = \frac{7}{2}$ separate distinct domains of behavior in this system, and the scattering angle diverges as ρ approaches these values. In a dynamical system, such domains of behavior are typically bounded by separatrices: manifolds dividing initial conditions with different dynamical behavior. No separatrices are identified in these prior studies, and the purpose of the present paper is to find them and see how they illuminate the phenomenon. To do so, we first introduce a sequence of transformations that will allow us to compute and visualize these separatrices.

3. Reduction by stages

Choosing the proper coordinate system may significantly clarify the study of a particular phenomenon, but how to construct such a coordinate system may not be obvious. In the ideal case, any such coordinates should be easy to interpret, which implies, among other things, that they should have a clear meaning and be invertible so that we may reconstruct the original motion from the transformed motion. We are particularly interested in *canonical* changes of variables, those which preserve the Hamiltonian form of the evolution equations. The first change of variables to Jacobi coordinates is canonical, while the second change, a Nambu reduction, requires us to generalize the framework of Hamiltonian systems.

Müller and Névir showed that Gröbli's reduced equations could be reinterpreted as Nambu dynamics [24], but this construction does not solve the problem of those coordinates' singularity.

3.1. **Jacobi coordinate reductions.** Jacobi coordinates are a standard tool for reducing n-body problems, especially in celestial mechanics, and are discussed at length in Jacobi's 1866 Lectures on

Dynamics [18]. It is a straightforward method and underlies the reductions used in many studies of vortex interactions [29]. Still, the point-vortex paper we have found that references the method by name is a recent one by Luo et al. [21].

The Jacobi coordinate transformation consists of iteratively applying the change of variables

$$\tilde{\mathbf{r}}_1 = \mathbf{r}_1 - \mathbf{r}_2; \qquad \tilde{\Gamma}_1 = \frac{\Gamma_1\Gamma_2}{\Gamma_1+\Gamma_2}; \tag{3.1}$$

$$\tilde{\mathbf{r}}_2 = \frac{\Gamma_1\mathbf{r}_1+\Gamma_2\mathbf{r}_2}{\Gamma_1+\Gamma_2}; \qquad \tilde{\Gamma}_2 = \Gamma_1+\Gamma_2, \tag{3.2}$$

where $\Gamma_1+\Gamma_2 \neq 0$. The variables $\tilde{\Gamma}_1$ and $\tilde{\Gamma}_2$, are known, respectively, as the *reduced circulation* and *total circulation* of the pair. These equations may be inverted to obtain the original coordinates

$$\mathbf{r}_1 = \tilde{\mathbf{r}}_2 + \frac{\Gamma_2}{\Gamma_1+\Gamma_2}\tilde{\mathbf{r}}_1, \quad \mathbf{r}_2 = \tilde{\mathbf{r}}_2 - \frac{\Gamma_1}{\Gamma_1+\Gamma_2}\tilde{\mathbf{r}}_1. \tag{3.3}$$

Substituting these back into the Hamiltonian (2.2) yields a new Hamiltonian $H(\tilde{\mathbf{r}}_1, \tilde{\mathbf{r}}_2, \mathbf{r}_3, \ldots, \mathbf{r}_N)$ and evolution equations of the form (2.3) with circulations $\tilde{\Gamma}_1, \tilde{\Gamma}_2, \Gamma_3, \ldots, \Gamma_N$. We then apply a similar transform to Eq. (3.1) to $\tilde{\mathbf{r}}_2$, $\mathbf{r}_3$, $\tilde{\Gamma}_2$ and Γ_3, repeating the process for each pair until $\mathbf{r}_N$ has been transformed. The transformed circulations redefine the Poisson bracket (2.4) and thus the evolution equations (2.5).

We assume that

$$\sum_{j=0}^{N} \Gamma_j \neq 0, \tag{3.4}$$

and, moreover, that the vortex labels have been chosen to ensure that

$$\sum_{j=0}^{k} \Gamma_j \neq 0, \text{ for all } k \leq N. \tag{3.5}$$

Condition (3.5) ensures that this will be possible at each state. Because the mass of the jth body, which serves as the analog to the circulation Γ_j, must be positive, condition (3.5) is never an issue in the gravitational problem.

We now discuss the meanings of these coordinates. We assign the names $\mathbf{R}_j$ to the transformed variables and κ_j to the transformed circulations. Clearly, $\mathbf{R}_1$ is the displacement from $\mathbf{r}_2$ to $\mathbf{r}_1$ and, similarly, $\mathbf{R}_2$ is the displacement from $\mathbf{r}_3$ to the center of vorticity of the $\mathbf{r}_1$, $\mathbf{r}_2$ subsystem. A similar definition holds for the remaining $\mathbf{R}_j$ with $j < N$, whereas $\mathbf{R}_N$ coincides with our previously defined $\mathbf{r}_0$, the center of vorticity defined in Eq. (2.10). Since this quantity is conserved, we have reduced the dimension of the phase space by two.

We now apply this change of variables to the three-vortex system defined by Hamiltonian (2.11). The transformed positions and circulations are

$$\begin{aligned} \mathbf{R}_1 &= \mathbf{r}_1 - \mathbf{r}_2; & \kappa_1 &= \frac{1}{2}; \\ \mathbf{R}_2 &= \frac{\mathbf{r}_1+\mathbf{r}_2}{2} - \mathbf{r}_3; & \kappa_2 &= -2; \\ \mathbf{R}_3 &= \mathbf{r}_1 + \mathbf{r}_2 - \mathbf{r}_3; & \kappa_3 &= 1. \end{aligned} \tag{3.6}$$

Because $\mathbf{R}_3$ is simply the conserved center of vorticity $\mathbf{r}_0$, we may without loss of generality set

$$\mathbf{R}_3 = \mathbf{r}_0 = 0. \tag{3.7}$$

In these coordinates, the Hamiltonian and angular impulse are

$$H = -\frac{1}{2}\log\|\mathbf{R}_1\|^2 + \frac{1}{2}\log\left\|\mathbf{R}_2 + \frac{\mathbf{R}_1}{2}\right\|^2 + \frac{1}{2}\log\left\|\mathbf{R}_2 - \frac{\mathbf{R}_1}{2}\right\|^2, \tag{3.8}$$

and

$$\Theta = \frac{1}{2}\|\mathbf{R}_1\|^2 - 2\|\mathbf{R}_2\|^2. \tag{3.9}$$

3.2. **Further reduction via Nambu brackets.** Before further reducing the equations, we normalize the system using Eq. (2.6) and the values of κ_j from Eq. (3.6), which gives

$$\begin{aligned} Q_1 &= \frac{1}{\sqrt{2}}X_1, \quad P_1 = \frac{1}{\sqrt{2}}Y_1, \\ Q_2 &= \sqrt{2}X_2, \quad P_2 = -\sqrt{2}Y_2. \end{aligned} \tag{3.10}$$

Defining $\mathcal{R}_i = \langle Q_i, P_i\rangle$ and $\bar{\mathcal{R}}_i = \langle Q_i, -P_i\rangle$, the conserved quantities become (up to an additive constant)

$$H = -\frac{1}{2}\log\|\mathcal{R}_1\|^2 + \frac{1}{2}\log\left\|\mathcal{R}_1 + \bar{\mathcal{R}}_2\right\|^2 + \frac{1}{2}\log\left\|\mathcal{R}_1 - \bar{\mathcal{R}}_2\right\|^2, \tag{3.11}$$

and

$$\Theta = \|\mathcal{R}_1\|^2 - \|\mathcal{R}_2\|^2. \tag{3.12}$$

Finally, we introduce a change of variables that allows us to express the dynamics using Nambu brackets [15–17, 25].

$$\begin{aligned} Z &= \|\mathcal{R}_1\|^2 + \|\mathcal{R}_2\|^2, \\ X + iY &= 2\mathcal{R}_1\mathcal{R}_2, \end{aligned} \tag{3.13}$$

where $\mathcal{R}_i$ are allowed to multiply as if they were complex variables with real and imaginary parts Q_i and P_i. These coordinates satisfy

$$\Theta^2 = Z^2 - X^2 - Y^2, \tag{3.14}$$

which we know to be conserved. Thus, the trajectory $(X(t), Y(t), Z(t))$ is confined to the upper sheet of a hyperbola of two sheets, which degenerates to a cone when $\Theta = 0$. Because $Z \geq 0$ by definition, the trajectories lie on the upper sheet.

In these variables, the Hamiltonian is just

$$H = -\frac{1}{2}\log(Z + \Theta) + \frac{1}{2}\log\left(Z^2 - X^2\right). \tag{3.15}$$

The *Nambu bracket* of three functions $F(X, Y, Z)$, $G(X, Y, Z)$, and $K(X, Y, Z)$ may be defined as

$$\{F, G, K\} = \boldsymbol{\nabla}F \cdot (\boldsymbol{\nabla}G \times \boldsymbol{\nabla}K). \tag{3.16}$$

Then one may show that the dynamics due to the Hamiltonian (3.11) and Poisson bracket (2.8) under the evolution law (2.5) are equivalent to allowing X, Y, and Z to evolve according to

$$\dot{F} = \{F, 2\Theta, H\}, \tag{3.17}$$

i.e.,

$$\frac{\mathrm{d}X}{\mathrm{d}t} = \qquad + 4Z\frac{\partial H}{\partial Y} + 4Y\frac{\partial H}{\partial Z}; \tag{3.18a}$$

$$\frac{\mathrm{d}Y}{\mathrm{d}t} = -4Z\frac{\partial H}{\partial X} \qquad - 4X\frac{\partial H}{\partial Z}; \tag{3.18b}$$

$$\frac{\mathrm{d}Z}{\mathrm{d}t} = -4Y\frac{\partial H}{\partial X} + 4X\frac{\partial H}{\partial Y}. \tag{3.18c}$$

While significant mathematical structure underlies this transformation, this calculation is simply a long exercise in using the chain rule.

For the conserved quantities (3.15) and (3.14), this gives evolution equations

$$\frac{\mathrm{d}X}{\mathrm{d}t} = \frac{-2Y}{Z+\Theta} + \frac{4ZY}{Z^2 - X^2}; \tag{3.19a}$$

$$\frac{\mathrm{d}Y}{\mathrm{d}t} = \frac{2X}{Z+\Theta}; \tag{3.19b}$$

$$\frac{\mathrm{d}Z}{\mathrm{d}t} = \frac{4XY}{Z^2 - X^2}. \tag{3.19c}$$

This is the main reduced form we will use to analyze this system. Unlike Gröbli's side length equations, system (3.19) is only singular at the singularities of Hamiltonian (2.2).

3.3. **An interpretation of the final coordinate system.** We now provide a simple geometric interpretation relating the (X, Y, Z, Θ) coordinate system to the physical coordinates. Consider Figure 3.1. By assumption (2.10), the center of vorticity lies at the origin, and we let $\mathbf{v}_j$ denote the vector from the origin to vortex j. Relation (2.10) implies that $\mathbf{v}_3 = \mathbf{v}_1 + \mathbf{v}_2$ so that the positions of the three vortices and the origin form a parallelogram, a fact mentioned by Gröbli [14, §3]. We let ϕ be the angle from $\mathbf{v}_1$ to $\mathbf{v}_2$. We then find by following through the sequence of changes of variables that

$$\begin{aligned} X &= -\|\mathbf{v}_1\|^2 + \|\mathbf{v}_2\|^2; \\ Y &= 2\,(\mathbf{v}_1 \times \mathbf{v}_2)\cdot\mathbf{k} = 2\|\mathbf{v}_1\|\|\mathbf{v}_2\|\sin\phi; \\ Z &= \quad\|\mathbf{v}_1\|^2 + \|\mathbf{v}_2\|^2; \\ \Theta &= -2\,\mathbf{v}_1\cdot\mathbf{v}_2 = -2\|\mathbf{v}_1\|\|\mathbf{v}_2\|\cos\phi. \end{aligned} \tag{3.20}$$

Now that we know the simple relation between the original coordinate system and the (X, Y, Z, Θ) coordinates, it may be tempting to skip over the reduction procedure used here and simply state that a useful and straightforward coordinate system has been found. Nonetheless, writing out the steps taken is instructive and will help generalize this calculation below.

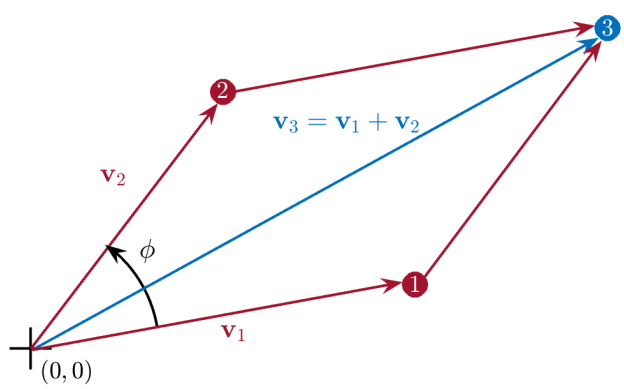

FIGURE 3.1. Diagram used to interpret the (X, Y, Z, Θ) coordinates. See the text for an explanation.

Some observations

- X is the signed difference between the lengths of $\mathbf{v}_1$ and $\mathbf{v}_2$, so vanishes when the triangle of vortices is isosceles.

- Y vanishes when the three vortices are collinear, which is not a singularity of the coordinate system.
- For $\Theta = 0$, $\cos\phi = 0$, so at all times, the three vortices form a right triangle, with vortex 2 at the right angle. Then, trivially, they cannot be collinear, so $Y \neq 0$; this can also be deduced from the singularity of the Hamiltonian (3.15) when $\Theta = 0$.

3.4. **Recovering some angles.** The argument above shows that the (X, Y, Z, Θ) variables are insensitive to a rigid rotation of the parallelogram in Fig. 3.1 about the origin. Therefore, we introduce a canonical form of polar coordinates (the action-angle variables of a harmonic oscillator) to recover this angle.

Returning to the coordinates $\mathcal{R}_1$ and $\mathcal{R}_2$ used in Eq. (3.11), we let

$$\mathcal{R}_1 = \langle \sqrt{2I_1}\sin\theta_1, \sqrt{2I_1}\cos\theta_1 \rangle, \quad \mathcal{R}_2 = \langle \sqrt{2I_2}\sin\theta_2, \sqrt{2I_2}\cos\theta_2 \rangle. \tag{3.21}$$

Two observations are important here. First, the Hamiltonian depends on the angles only through the combination $\theta_1 + \theta_2$. Second, the vector $\mathbf{v}_3$ in the figure has argument $\theta_2 - \frac{\pi}{2}$. Therefore, we make one additional canonical transformation

$$\psi_1 = \theta_1 + \theta_2, \quad \psi_2 = \theta_2, \quad J_1 = I_1, \quad J_2 = I_2 - I_1, \tag{3.22}$$

In these variables, the Hamiltonian takes the form (again ignoring additive constants)

$$H = \frac{1}{2}\log\left(4J_1^2\sin^2\psi_1 + 4J_1J_2\sin^2\psi_1 + J_2^2\right) - \frac{1}{2}\log\left(J_1\right) \tag{3.23}$$

Since the equation is cyclic in ψ_2, the action $J_2 = -\Theta/2$ is conserved. The dynamics of J_1 and ψ_1 are equivalent to system (3.19). We may recover the evolution of $\theta_2 = \psi_2$ by integrating

$$\dot{\psi}_2 = \frac{2J_1\sin^2\psi_1 + J_2}{4J_1^2\sin^2\psi_1 + 4J_1J_2\sin^2\psi_1 + J_2^2} \tag{3.24}$$

along a scattering trajectory. In terms of the Nambu variables, this becomes

$$\dot{\theta}_2 = \frac{2Y^2\sqrt{\Theta^2 + X^2 + Y^2} - 2\Theta X^2}{(X^2 + Y^2)(\Theta^2 + Y^2)}. \tag{3.25}$$

The angle just calculated describes the argument of $\mathbf{v}_3$ in Fig. 3.1, which is distinct from the scattering angle $\alpha = \arg\frac{\mathrm{d}z_3}{\mathrm{d}t}$ plotted in Fig 2.2. In terms of the reduced coordinates, we find that

$$\frac{\mathrm{d}\alpha}{\mathrm{d}t} = -\frac{8\Theta Y^2}{(X^2 + Y^2)(\Theta^2 + Y^2)}. \tag{3.26}$$

Integrating this over a trajectory then gives $\Delta\alpha$.

4. Analysis and visualization of the reduced system

We first derive the fixed points and singularities of system (3.19) before visualizing the system's phase space.

4.1. **Fixed points and singularities.** To find fixed points, we the right-hand sides of system (3.19) to zero while enforcing the constraints (3.14) and $Z \geq 0$. Similarly, the system has singularities where either term in the Hamiltonian (3.15) vanishes, enforcing the same two constraints. Which equilibria and singularities exist depends on Θ.

When $\Theta < 0$, the system has two equilibria $\mathcal{E}_{\text{tri}}^{\pm}$ and a singularity $\mathcal{S}_{11}$ found by setting $Z + \Theta = 0$, which requires $X = Y = 0$.

$$\mathcal{E}_{\text{tri}}^{\pm} = \begin{pmatrix} X_\pm \\ Y_\pm \\ Z_\pm \end{pmatrix} = \begin{pmatrix} 0 \\ \pm\sqrt{3}\Theta \\ -2\Theta \end{pmatrix} \quad \text{and} \quad \mathcal{S}_{11} = \begin{pmatrix} 0 \\ 0 \\ -\Theta \end{pmatrix}. \tag{4.1}$$

When $\Theta = 0$, there are no equilibria, but the system is singular when $Z = |X|$, which requires $Y = 0$.

When $\Theta > 0$, the system has a single equilibrium

$$\mathcal{E}_{-1} \equiv \begin{pmatrix} X_0 \\ Y_0 \\ Z_0 \end{pmatrix} = \begin{pmatrix} 0 \\ 0 \\ \Theta \end{pmatrix} \tag{4.2}$$

and no singularities.

The fixed points $\mathcal{E}^{\pm}_{\text{tri}}$ and $\mathcal{E}_{-1}$ are *relative equilibria* in the laboratory coordinates, i.e., they are equilibria when viewed in an appropriate rotating reference frame. We may interpret them using Eq. (3.20). For both equilibria $X = 0$ implies $\|\mathbf{v}_1\| = \|\mathbf{v}_2\|$. The equilibrium $\mathcal{E}^{\pm}_{\text{tri}}$ exists for $\Theta < 0$. For the equilibrium $\mathcal{E}^{\pm}_{\text{tri}}$, the value of the component $Z = -2\Theta$ implies that $\phi = \pm\frac{\pi}{3}$ and the three vortices lie at the vertices of an equilateral triangle, motivating the naming convention. The equilibrium $\mathcal{E}_{-1}$ exists for $\Theta > 0$. This implies $\phi = \pi$ so that the three vortices are collinear with the two positive vortices equally spaced from the negative vortex at the center. The subscript -1 indicates that the vortex with circulation -1 sits at the center. By similar reasoning, we find that at the singularity $\mathcal{S}_{11}$, the two vortices with circulation $+1$ coincide, again motivating the notation.

4.2. **The phase space.** By the conservation law (3.14), the phase space of system (3.19) is the upper sheet of a two-sheeted hyperbola. We visualize the dynamics by projecting this surface into the XY plane in Fig. 4.1. The conserved angular impulse Θ plays the role of a bifurcation parameter, but up to scaling when $\Theta \neq 0$, there are only three possible phase planes.

For $\Theta < 0$ in panel (a), the point at the origin is the singularity $\mathcal{S}_{11}$. The two equilibria $\mathcal{E}^{\pm}_{\text{tri}}$ sit on the Y axis and are seen to be saddle points connected by a pair of homoclinic orbits. The two homoclines surround a family of periodic orbits, which shrink to a point at $\mathcal{S}_{11}$. Each corresponds to a hierarchical orbit in which the two positive vortices orbit about each other rapidly while their mutual center of vorticity and the third vortex orbit each other; Gröbli computed this orbit in closed form and plotted it [14, Fig. 1]. As the diameter of these closed orbits goes to zero, the rotation rate of this tightly bound pair diverges, and the orbits approach the singularity $\mathcal{S}_{11}$. The unbounded portions of the stable and unstable manifolds separate the remainder of the phase plane into four unbounded quadrants. This will be important when we return to discuss the scattering problem.

When $\Theta = 0$ in panel (b), the entire X axis is singular, and all solutions are confined to the upper or lower half-planes. For $\Theta > 0$ in panel (c), the collinear equilibrium $\mathcal{E}_{-1}$ at the origin is a saddle point. Its invariant manifolds also separate the plane into four unbounded quadrants.

Finally, note that rescaling X and Y by $|\Theta|$ and t by $|\Theta|^{-1}$ (when $\Theta \neq 0$) shows that the dynamics for any negative (respectively, positive) value of Θ has a phase plane equivalent to that shown in the left (respectively, right) subfigure.

4.3. **Explaining the scattering.** We now explain the behavior of the three-vortex scattering problem depicted in Fig. 2.1. The critical insight of the pendulum example is that the stable and unstable manifolds of the inverted equilibrium form boundaries, or *separatrices*, between different types of dynamics. In that system, the periods diverge as one moves between curves along either family of periodic orbits toward a separatrix. In the vortex system, the most likely explanation for the change in behavior from direct scattering to exchange scattering and back at $\rho = -1$ and $\rho = \frac{7}{2}$, and the divergence of the scattering angle near these points seem likely to depend on the crossing of separatrices. That is indeed the case, as we now show.

The separatrices shown in Fig. 4.1 divide the phase plane into families of trajectories with identical topology, and the topology of the phase plane is determined, in turn, by the conserved

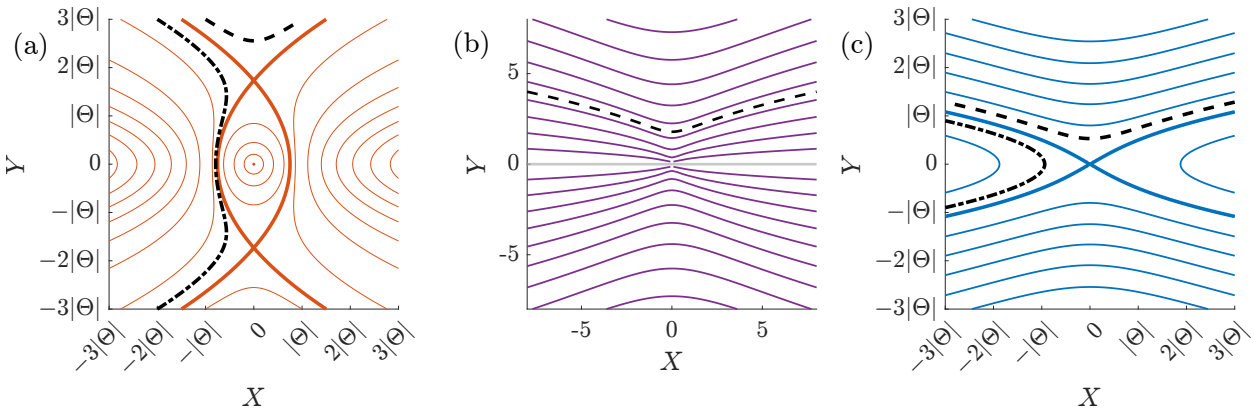

FIGURE 4.1. The XY phase planes of system (3.19). (a) The case $\Theta < 0$ with singularity $\mathcal{S}_{11}$ (point) and triangular configurations at the intersections of the thick curves. (b) The case $\Theta = 0$. The gray line $Y = 0$ is singular. (c) the case $\Theta > 0$ with collinear equilibrium $\mathcal{E}_{-1}$. Note that the contours are not evenly-spaced level sets of the energy (3.15) but were chosen to illustrate the topology clearly.

parameter Θ. Panel (a) depicts the case $\Theta < 0$, where the energy level of the separatrices equals that of the rotating triangular configurations $\mathcal{E}^{\pm}_{\text{tri}}$, given by

$$E(\mathcal{E}^{\pm}_{\text{tri}}) = \frac{1}{2}\log(-4\Theta). \tag{4.3}$$

The energy in the two regions to the left and right of $\mathcal{E}^{\pm}_{\text{tri}}$ (those containing the X-axis) is lower than $E(\mathcal{E}_{-1})$, while the energy in the regions above and below the separatrices is higher than $E(\mathcal{E}^{\pm}_{\text{tri}})$.

Panel (c) shows the case $\Theta > 0$, where the energy level on the separatrices equals that of the collinear equilibrium $\mathcal{E}_{-1}$, which we compute to be

$$E(\mathcal{E}_{-1}) = \frac{1}{2}\log\frac{\Theta}{2}. \tag{4.4}$$

The energy in the two regions to the left and right of $\mathcal{E}_{-1}$ (those containing the X-axis) is lower than $E(\mathcal{E}_{-1})$, while the energy in the regions above and below the separatrices is higher than $E(\mathcal{E}_{-1})$.

We must compare these energies with those of the pre-scattering condition depicted in Fig. 2.1. In this arrangement, the center of vorticity is at the origin, so we may compute the limiting behavior of X and Y using the equations in (3.20). We directly compute that, independent of L,

$$\Theta = 1 + 2\rho. \tag{4.5}$$

We assume that as $t \to -\infty$, $L \to \infty$, thus $\|\mathbf{v}_1\| \to \infty$ while $\|\mathbf{v}_2\|$ is finite, so that $X \to -\infty$, this also implies that $Y \to \infty$. Thus, for the situation depicted in Fig. 2.1, trajectories in the phase planes depicted in Fig. 4.1 arrive from infinity from the northwest direction heading southeast.

Then, suppose the initial energy exceeds the separatrix energy. In that case, the trajectory begins above the separatrix and crosses the line $X = 0$, where $\frac{\mathrm{d}Y}{\mathrm{d}t} = 0$ before escaping to infinity in the northeast direction. Because $X \to +\infty$ as $t \to \infty$, $\|\mathbf{v}_2\|$ must diverge, and this is an exchange scattering event. At the instant the solution crosses $X = 0$, then $\|\mathbf{v}_1\| = \|\mathbf{v}_2\|$ at which point the vectors $\mathbf{v}_1$ and $\mathbf{v}_2$ form the legs of an iscosceles triangle.

If, instead, the initial energy lies below the separatrix energy, then the trajectory begins below the separatrix. It will cross $Y = 0$ at which point $\frac{\mathrm{d}X}{\mathrm{d}t}$ =0. When $Y = 0$, then $\sin\phi = 0$, and the three vortices are collinear. Because $X < 0$ along the entire trajectory and $X \to \infty$ as $t \to \infty$, then $\|\mathbf{v}_1\| \to \infty$ and this solution represents a direct scattering event.

For $\Theta < 0$, that is, for $\rho < -\frac{1}{2}$, the critical energy is given by Eq. (4.3), which, combined with Eq. (4.5) gives a critical energy

$$\rho^-_{\text{crit}} = -1. \tag{4.6}$$

For $\Theta > 0$, that is, for $\rho > -\frac{1}{2}$, the critical energy is given by Eq. (4.4), which, combined with Eq. (4.5) gives a critical energy

$$\rho^+_{\text{crit}} = \frac{7}{2}. \tag{4.7}$$

Fig. 2.2 shows the deflection in the angle of vortex 2 following the interaction is singular as $\rho \to -1$ and $\rho \to \frac{7}{2}$ as expected.

To calculate the scattering angle, we must integrate Eq. (3.26) over each scattering trajectory. This is equivalent to a calculation by Lydon et al. [22], and we defer it to Appendix A.

We end this section by remarking that the values $\rho = 1$ ($\Theta = -1$), $\rho = -\frac{1}{2}$ ($\Theta = 0$), and $\rho = \frac{7}{2}$ ($\Theta = 8$) divide the space of initial conditions into four intervals on which the behavior is qualitatively distinct. Gröbli made the same observation (using a constant $\lambda = \Theta/2$) as did Lydon et al. [14, 22], but without reference to a phase plane to organize the orbits. Because both prior works focus on integrating the ODE system via quadrature, these intervals are distinguished mainly by the change in the algebraic forms of those integrals rather than the phase space topology.

The approach taken here is especially illuminating for the transition at $\Theta = 0$, for which there is an algebraic change in the form of the integrals but no visible discontinuity in the scattering angle in Fig. 2.2. We discuss this further next.

4.4. **The borderline case $\Theta = 0$.** Clearly, then, the critical values of ρ separating exchange scattering from direct scattering are those for which the energy of the initial condition as $L \to \infty$ equals that of the separatrices, i.e., the energy of the hyperbolic fixed points. From Eq. (4.5), we see

$$\Theta > 0 \quad \text{for} \quad \rho > -\frac{1}{2} \quad \text{and} \quad \Theta < 0 \quad \text{for} \quad \rho < -\frac{1}{2}. \tag{4.8}$$

The singular case $\Theta = 0$, when the conservation law (3.20) confines the dynamics to a cone, therefore corresponds to $\rho = -\frac{1}{2}$. The schematic in Fig. 2.1, which is defined for finite L, is somewhat misleading, as the trajectories of all three vortices lie along straight lines parallel to the line connecting vortices 1 and 3 in the figure and are not horizontal. Rotating the coordinate system so that the trajectories are horizontal, we find that

$$\begin{aligned} x_1 &= \frac{t - \sqrt{t^2+4}}{2}, & x_2 &= \frac{t + \sqrt{t^2+4}}{2}, & x_3 &= t; \\ y_1 &= -1, & y_2 &= -1, & y_3 &= -2. \end{aligned}$$

The dynamics of this case are shown in Fig. 4.2 and were known to Gröbli [14, §4]. Vortex 1 slows down and comes to rest at $x = 0$, transferring its energy to vortex 2.

5. Generalization to $\Gamma_2 \neq 1$

In this section, we will generalize to the case in which $\Gamma_1 = -\Gamma_3 = 1$ but $0 < \Gamma_2 = \Gamma \neq 1$, i.e., the case when the remaining vortex has a distinct positive circulation. Exchange scattering is no longer possible since vortices 2 and 3 can no longer form a dipole and escape. Consequently, some bifurcation must reconfigure the phase plane dynamics depicted in Fig. 4.1. To determine how this bifurcation occurs, we must first generalize the reduction that led to ODE system (3.19).

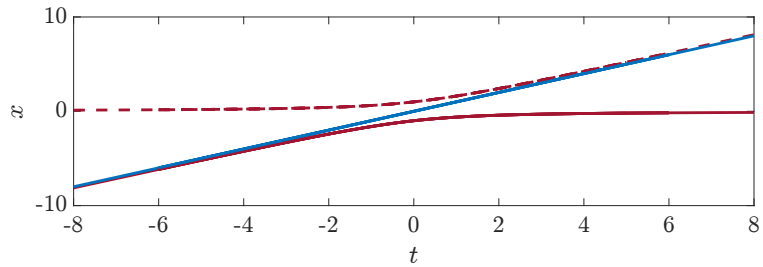

FIGURE 4.2. The x-component of the solution for $\rho = 0$, corresponding to a trajectory in the middle phase plane of Fig. 4.1.

5.1. **The reduction for $\Gamma_2 \neq 1$.** We will make the canonical change of variables in two steps. The first transformation recombines vortex $\mathbf{r}_1$ and $\mathbf{r}_2$, so that $\mathbf{r}_3$ and Γ_3 are unchanged.

The second transformation recombines vortex $\tilde{\mathbf{r}}_2$ and $\tilde{\mathbf{r}}_3$, so that $\tilde{\mathbf{r}}_1$ and $\tilde{\Gamma}_1$ are unchanged,

$$\begin{aligned} \mathbf{R}_1 &= \tilde{\mathbf{r}}_1; & \kappa_1 &= \tilde{\Gamma}_1 = \frac{\Gamma}{\Gamma+1}; \\ \mathbf{R}_2 &= \tilde{\mathbf{r}}_2 - \tilde{\mathbf{r}}_3; & \kappa_2 &= \frac{\tilde{\Gamma}_2\tilde{\Gamma}_3}{\tilde{\Gamma}_2+\tilde{\Gamma}_3} = -\frac{1+\Gamma}{\Gamma}; \\ \mathbf{R}_3 &= \frac{\tilde{\Gamma}_2\tilde{\mathbf{r}}_2 + \tilde{\Gamma}_3\tilde{\mathbf{r}}_3}{\tilde{\Gamma}_2+\tilde{\Gamma}_3}; & \kappa_3 &= \tilde{\Gamma}_2 + \tilde{\Gamma}_3 = \Gamma. \end{aligned} \tag{5.1}$$

As before, we may set $\mathbf{R}_3 = 0$. Simplifying the coordinate transformation yields

$$\mathbf{R}_1 = \mathbf{r}_1 - \mathbf{r}_2; \quad \mathbf{R}_2 = -\frac{\Gamma}{1+\Gamma}\left(\mathbf{r}_1 + \Gamma\mathbf{r}_2\right). \tag{5.2}$$

In these coordinates, the generalized Hamiltonian and angular impulses are

$$H = -\frac{\Gamma}{2}\log\|\mathbf{R}_1\|^2 + \frac{\Gamma}{2}\log\left\|\frac{\mathbf{R}_1}{1+\Gamma}\right\|^2 - \mathbf{R}_2 + \frac{1}{2}\log\left\|\frac{\Gamma}{1+\Gamma}\mathbf{R}_1 + \mathbf{R}_2\right\|, \tag{5.3}$$

and

$$\Theta = \kappa_1\|\mathbf{R}_1\|^2 + \kappa_2\|\mathbf{R}_2\|^2 \quad (\text{note } \kappa_2 < 0). \tag{5.4}$$

The normalization (2.6), now takes the form

$$\begin{aligned} Q_1 &= \sqrt{\kappa_1}X_1, & P_1 &= \sqrt{\kappa_1}Y_1, \\ Q_2 &= \sqrt{-\kappa_2}X_2, & P_2 &= -\sqrt{-\kappa_2}Y_2. \end{aligned} \tag{5.5}$$

Using these to define the coordinates $\mathcal{R}_i$ and $\bar{\mathcal{R}}_i$, the Hamiltonian reduces to (up to an additive constant)

$$H = -\frac{\Gamma}{2}\log\|\mathcal{R}_1\|^2 + \frac{\Gamma}{2}\log\left\|\Gamma\bar{\mathcal{R}}_2 - \mathcal{R}_1\right\|^2 + \frac{1}{2}\log\left\|\bar{\mathcal{R}}_2 + \mathcal{R}_1\right\|^2. \tag{5.6}$$

The conserved angular impulse reduces again to (3.9). We may again define coordinates X, Y, and Z using Eq. (3.13), and the relation (3.14) still holds. Using these definitions the Hamiltonian (5.6) is given by:

$$H(X,Y,Z,\Theta) = \frac{\Gamma}{2}\log\big(Z(\Gamma^2+1) + (1-\Gamma^2)\Theta - 2\Gamma X\big) - \frac{\Gamma}{2}\log(Z+\Theta) + \frac{1}{2}\log(Z+X). \tag{5.7}$$

As in Sec. 3.3, we may interpret the relationship between the (X,Y,Z,Θ) coordinates and the laboratory frame. However, the results are less tidy, so we make a few remarks instead. By definition, the variable Z remains positive, and $Y = 0$ whenever the three vortices are collinear. It is

no longer the case that the triangle is isosceles when $X = 0$. However, $X \to -\infty$ as $\|\mathbf{r}_2 - \mathbf{r}_3\| \to \infty$ and $X \to +\infty$ as $\|\mathbf{r}_1 - \mathbf{r}_2\| \to \infty$. This last observation allows us to discriminate between direct and exchange scattering.

By applying Eqs. (3.16) and (3.17) to the Hamiltonian (5.7) and the conserved quantity (3.14), and using Eqs. (3.18), the system evolves according to

$$\frac{\mathrm{d}X}{\mathrm{d}t} = \frac{2\Gamma Y}{Z+\Theta} - \frac{2Y}{X+Z} - \frac{2\Gamma(1+\Gamma^2)Y}{(\Gamma^2+1)Z + (1-\Gamma^2)\Theta - 2\Gamma X}; \tag{5.8a}$$

$$\frac{\mathrm{d}Y}{\mathrm{d}t} = 2 - \frac{2\Gamma X}{Z+\Theta} + \frac{2\Gamma(1+\Gamma^2)X - 4\Gamma^2 Z}{Z(\Gamma^2+1) + (1-\Gamma^2)\Theta - 2\Gamma X}; \tag{5.8b}$$

$$\frac{\mathrm{d}Z}{\mathrm{d}t} = \frac{2Y}{Z+X} - \frac{4\Gamma^2 Y}{Z(\Gamma^2+1) + (1-\Gamma^2)\Theta - 2\Gamma X}. \tag{5.8c}$$

5.2. **The phase space for $\Gamma_2 \neq 1$.** The equilibria of (5.8), which must satisfy both $Z > 0$ by (3.13) and satisfy the constraint (3.14) are:

$$\mathcal{E}^{\pm}_{\mathrm{tri}} = \Theta \begin{pmatrix} \frac{\Gamma(\Gamma-1)}{\Gamma+1} \\ \pm\sqrt{3}\Gamma \end{pmatrix}, \text{ for } \Theta < 0; \tag{5.9a}$$

$$\mathcal{E}_{-1} = \frac{\Gamma\Theta}{\Gamma^2-1} \begin{pmatrix} 1 - 2\Gamma^2 + \sqrt{4\Gamma^2 - 3} \\ 0 \end{pmatrix}, \text{ for } \Theta > 0 \text{ and } \Gamma > \frac{\sqrt{3}}{2}; \tag{5.9b}$$

$$\mathcal{E}_{\Gamma} = \frac{\Gamma\Theta}{\Gamma^2-1} \begin{pmatrix} 1 - 2\Gamma^2 - \sqrt{4\Gamma^2 - 3} \\ 0 \end{pmatrix}, \text{ for } \Theta > 0 \text{ and } \frac{\sqrt{3}}{2} < \Gamma < 1; \tag{5.9c}$$

$$\mathcal{E}_{1} = \frac{\Gamma\Theta}{\Gamma^2-1} \begin{pmatrix} 1 - 2\Gamma^2 - \sqrt{4\Gamma^2 - 3} \\ 0 \end{pmatrix}, \text{ for } \Theta < 0 \text{ and } \Gamma > 1. \tag{5.9d}$$

These last two are described by the same formula, but represent different vortex configurations and are defined for different parameter values. Only the X and Y coordinates are displayed; the Z coordinate is the positive solution to (3.14).

The system also has singularities at

$$\mathcal{S}_{1\Gamma} = \begin{pmatrix} 0 \\ 0 \end{pmatrix}, \text{ for } \Theta < 0 \text{ and } \Gamma > 0; \tag{5.10a}$$

$$\mathcal{S}_{-1\Gamma} = \begin{pmatrix} \frac{2\Gamma\Theta}{\Gamma^2-1} \\ 0 \end{pmatrix}, \text{ for } \Theta(\Gamma - 1) > 0. \tag{5.10b}$$

The dependence of the equilibria and singularities on Γ and Θ are most easily understood graphically using a bifurcation diagram, as shown in Fig. 5.1. Only the equilibria $\mathcal{E}^{\pm}_{\mathrm{tri}}$ and $\mathcal{E}_{-1}$ and the singularity $\mathcal{S}_{1\Gamma}$ exist for $\Gamma = 1$ and satisfy $\mathcal{S}_{1\Gamma} \to \mathcal{S}_{11}$ as $\Gamma \to 1$. They have the same physical meaning as discussed in Sec. 3.3. The other equilibria and singularities all satisfy $Y = 0$ and diverge $X \to +\infty$ as $\Gamma \to \pm 1$. The points $\mathcal{S}_{-1\Gamma}$, $\mathcal{E}_1$, and $\mathcal{E}_\Gamma$ all diverge to ∞ as $\Gamma \to 1^{\pm}$. The equilibria $\mathcal{E}_{-1}$ and $\mathcal{E}_\Gamma$ merge in a saddle-node bifurcation at $\Gamma = \frac{\sqrt{3}}{2}$.

The equilibria $\mathcal{E}_\Gamma$ and $\mathcal{E}_1$ correspond to collinear arrangements with the vortices of strength Γ and 1 in the middle, respectively. The singularity $\mathcal{S}_{-1\Gamma}$, corresponds to the limit of a family of hierarchical orbits in which vortices 2 and 3, with circulations Γ and -1, form a tight pair orbiting vortex 1 some distance away.

We now consider the phase space as Γ varies, again plotting the projection of the upper sheet of the hyperboloid onto the XY plane. First, we show the case $\Gamma > 1$ as shown in Fig. 5.2. For $\Theta < 0$, a collinear state $\mathcal{E}_1$ appears on the X-axis to the right of the region of closed orbits seen in Fig. 4.1, while for $\Theta > 0$ a new singular state $\mathcal{S}_{-1\Gamma}$ appears on the positive X-axis. Each of these

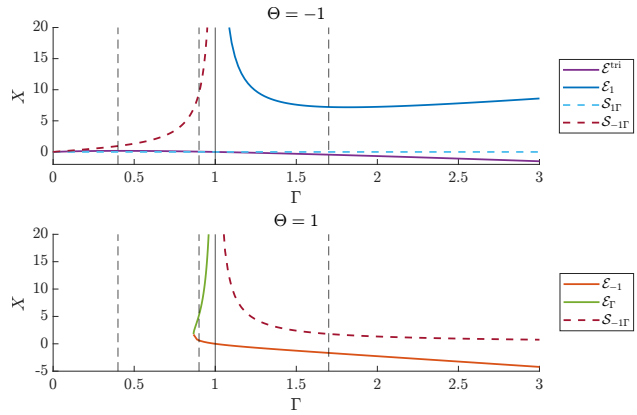

FIGURE 5.1. The X component of the equilibria (solid lines) and singularities (dashed lines) given in Eqs. (5.9) and (5.10). Figs. 4.1, 5.2, 5.4, and 5.5 show phase plane diagrams at the Γ values indicated by the vertical lines.

is surrounded by a family of periodic orbits that limit to a separatrix. In contrast with Fig. 4.1, all orbits in the right half plane cross the X-axis and do not extend to ∞.

The family of unbounded orbits corresponding to *exchange scattering* has been replaced by a family of orbits that cross the X-axis and approach infinity heading southwest. We call these *extended direct scattering* orbits. One such orbit with $\Gamma = 2$ is shown in Fig. 5.3. Remarkably, The coordinates of this trajectory, but not its time-parameterization, are given by Gröbli and displayed in the dissertation [14, Eqns (7.17), (7.19), and (7.20), and Fig. 5]. As $t \to \pm\infty$, vortices 1 and 3 form a dipole that moves along a nearly straight while vortex 2, but for a finite period of time, vortex 3 has changed partners, forming a dipole with vortex 2 and moving along a nearly circular orbit

Fig. 5.4 shows representative phase planes with $\frac{\sqrt{3}}{2} < \Gamma < 1$. While the topology in Figs. 5.2 and 5.4 looks the same, they differ in the kinds of singularities and fixed points. For $\Theta < 0$, the singularity $\mathcal{S}_{1\Gamma}$ remains unchanged from Fig. 5.2, while the equilibrium $\mathcal{E}_1$ to the right of the origin is replaced by a singularity $\mathcal{S}_{-1\Gamma}$. For $\Theta > 0$, the equilibrium $\mathcal{E}_{-1}$ is unchanged from Fig. 5.2, while the singular point $\mathcal{S}_{-1\Gamma}$ is replaced by the equilibrium $\mathcal{E}_\Gamma$.

Fig. 5.5 shows phase planes for $\Gamma < \frac{\sqrt{3}}{2}$. The phase plane for $\Theta < 0$ is equivalent to that in Fig. 5.4. However, the $\Theta > 0$ phase plane has changed significantly. At $\Gamma = \frac{\sqrt{3}}{2}$, the equilibria $\mathcal{E}_\Gamma$ and $\mathcal{E}_{-1}$ collide and annihilate in a saddle-node bifurcation, so the phase plane contains no equilibria or singularities. All the orbits for $\Theta > 0$ are of the direct scattering type.

5.3. **Explaining the scattering for $\Gamma \neq 1$.** We now explain the three-vortex scattering phenomenon in the generalized system. The setup remains as shown in Figure 2.1, except that $\Gamma_2 = \Gamma \neq 1$ and the two points forming the dipole are separated by a distance $\frac{d}{\Gamma}$ with positions $\mathbf{r}_1 = \langle -L, \rho + \frac{\Gamma d}{2} \rangle$, $\mathbf{r}_2 = \langle 0, -d \rangle$, and $\mathbf{r}_3 = \langle -L, \rho - \frac{\Gamma d}{2} \rangle$. We will again take $d = 1$. The generalized Hamiltonian and angular momentum in the new coordinates, $H \to \log(\Gamma)$ as $L \to +\infty$, and,

$$\Theta = \Gamma(1 + 2\rho).$$

To calculate the critical energy, we follow the process described in Section 4.3. For $\Theta < 0$, that is, for $\rho < -\frac{1}{2}$, the critical energy level remains the energy of the equilibra $\mathcal{E}^{\pm}_{\text{tri}}$. This again leads to the value $\rho^{-}_{\text{crit}} = -1$ given by Eq. (4.6). For $\Theta > 0$ and $\Gamma > \frac{\sqrt{3}}{2}$, the critical energy is again that of

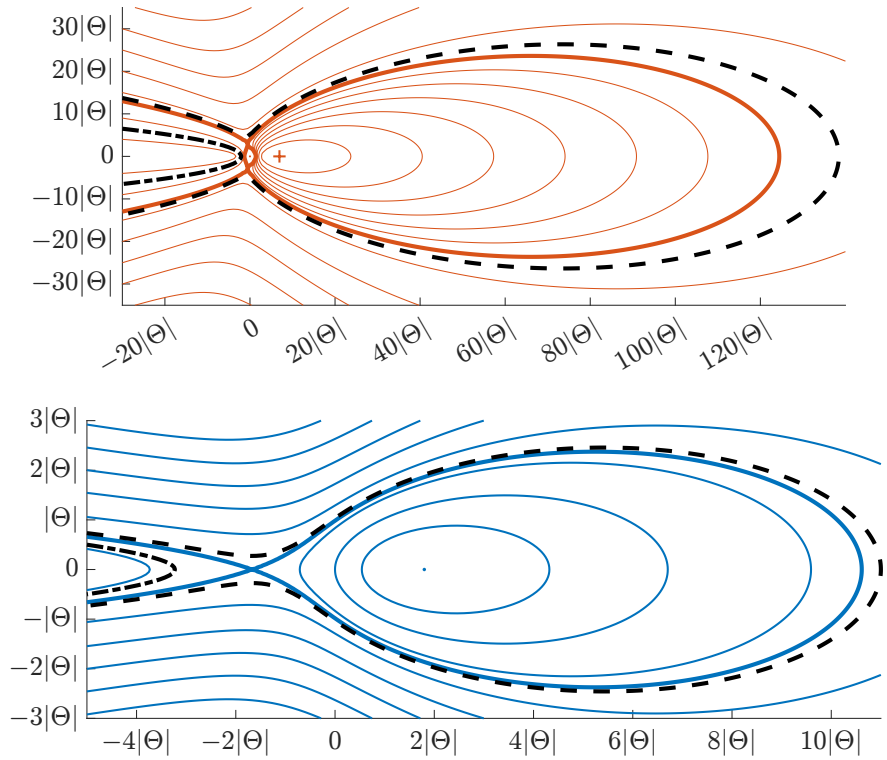

FIGURE 5.2. The phase planes for $\Gamma = 1.7 > 1$. Top: $\Theta < 0$ case showing the equilibria $\mathcal{E}_{\text{tri}}^{\pm}$ at the separatrix intersections, the singular point $\mathcal{S}_{1\Gamma}$ (point) and the collinear state $\mathcal{E}_1$ (+). Bottom: $\Theta > 0$ case with singular point $\mathcal{S}_{-1\Gamma}$ (point) and collinear state $\mathcal{E}_{-1}$ at the separatrix intersection.

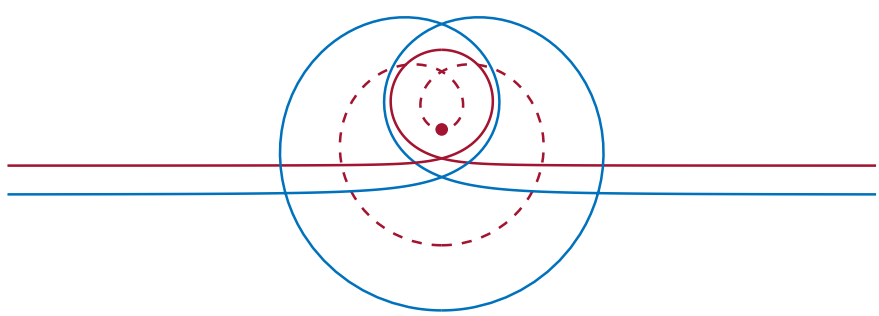

FIGURE 5.3. An extended direct scattering solution with $\Gamma = 2$ and $\rho = -\frac{9}{2}$. This is a direct simulation of a solution whose trajectory Gröbli computed in closed form.

the collinear equilibrium $\mathcal{E}_{-1}$

$$\rho_{\text{crit}}^{+} = \frac{1}{2}\left(\frac{\left(\left(\Gamma+1\right)\left(\Gamma^2-1\right)\right)\left(\frac{(B+1)(\Gamma+1)^2\left(\Gamma^2-1\right)}{-2A\Gamma^2+B(\Gamma^4-1)-(1-\Gamma^2)^2}\right)^{\Gamma}}{A\Gamma+B\left(\Gamma^2-1\right)}-1\right), \tag{5.11}$$

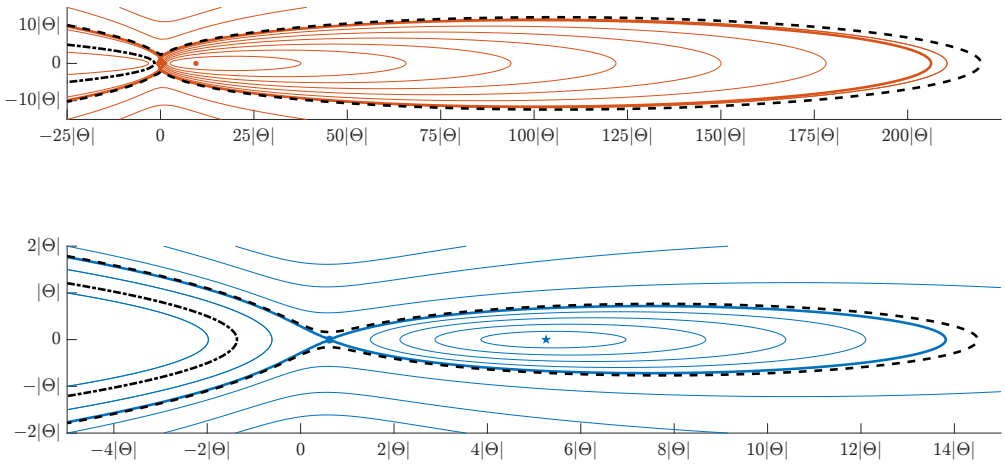

FIGURE 5.4. The phase planes for $\Gamma = 0.9 \in \left(\frac{\sqrt{3}}{2}, 1\right)$. Top: The $\Theta < 0$ case, showing two singular points, $\mathcal{S}_{1\Gamma}$ and $\mathcal{S}_{-1\Gamma}$ (points), and two equilibria $\mathcal{E}^{\pm}_{\text{tri}}$ at the separatrix intersections. Bottom: The $\Theta > 0$ case, showing collinear equilibria $\mathcal{E}_{\Gamma}$ ($\star$) and $\mathcal{E}_{-1}$ at the separatrix intersection.

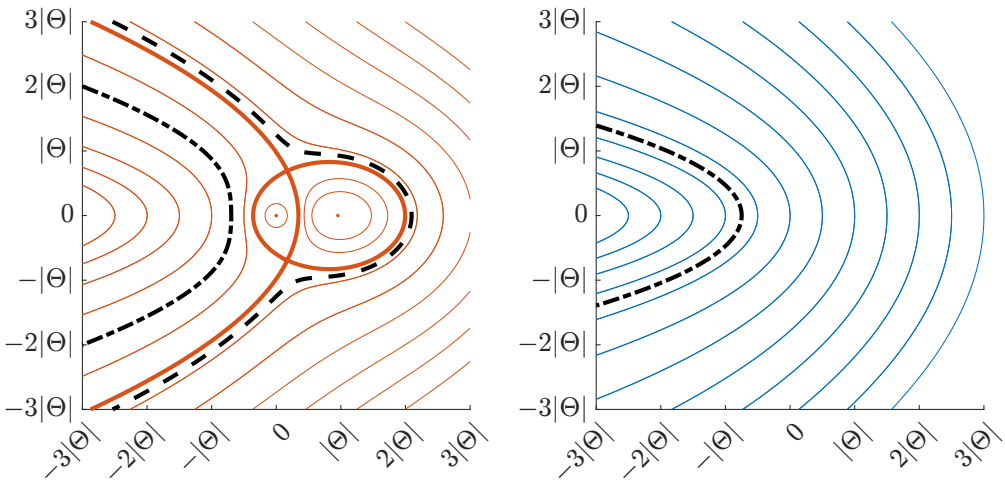

FIGURE 5.5. The phase planes for $\Gamma = 0.4 \in \left(0, \frac{\sqrt{3}}{2}\right)$. Left: The case $\Theta < 0$ with singular points $\mathcal{S}_{1\Gamma}$ (left) and $\mathcal{S}_{-1\Gamma}$ (right). Right: The case $\Theta > 0$, which has no fixed points or singular points.

where

$$A = 1 - 2\Gamma^2 + \sqrt{4\Gamma^2 - 3} \quad \text{and} \quad B = \sqrt{1 + \left(\frac{\Gamma A}{\Gamma^2 - 1}\right)^2}.$$

This matches the value $\frac{7}{2}$ given by (4.7) for $\Gamma = 1$. Since there is no hyperbolic fixed point when $\Theta > 0$ and $\Gamma < \frac{\sqrt{3}}{2}$, there should be only one singular point in the scattering diagram. Two such diagrams are shown in Fig. 5.6, demonstrating the disappearance of the second singularity for small Γ. For $\Gamma = 0.4$, the curve jumps by 2π at $\rho \approx -0.88$. This is explained by the disappearance of a loop in the path of vortex 3; see Fig. 5.7.

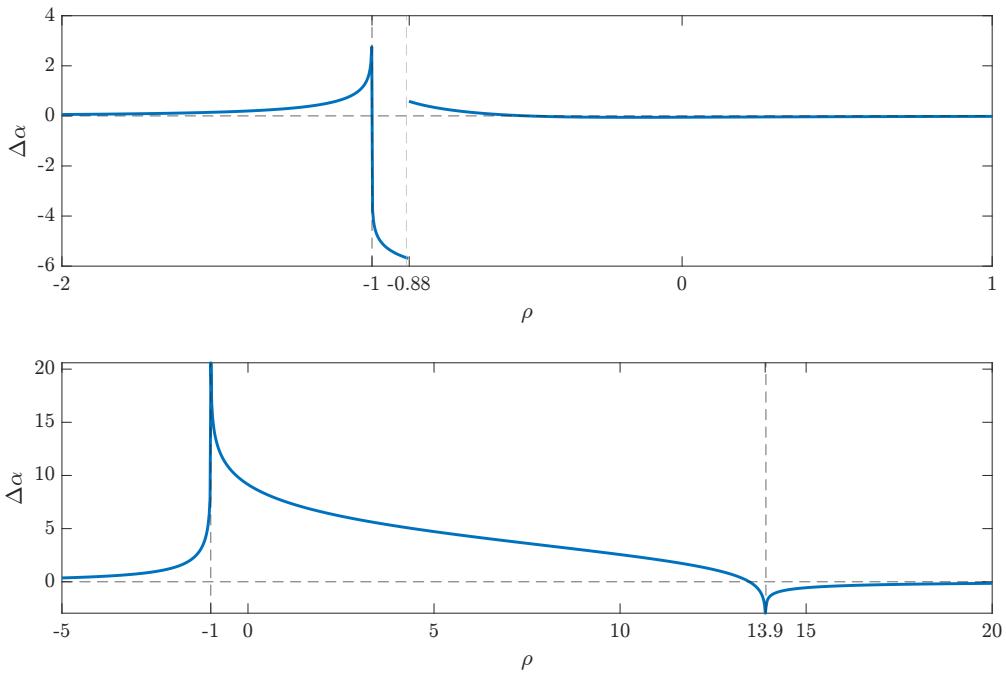

FIGURE 5.6. Top: The scattering angle as a function of ρ for $\Gamma = 0.4$, showing a singularity at $\rho = -1$, but without the second singularity. Instead, the curve jumps by 2π near $\rho = -0.88$, corresponding to the disappearance of a loop, as shown in Fig. 5.7. Bottom: The case $\Gamma = 1.7$ showing singularities at $\rho = -1$ and at $\rho \approx 13.9$, confirming formula (5.11).

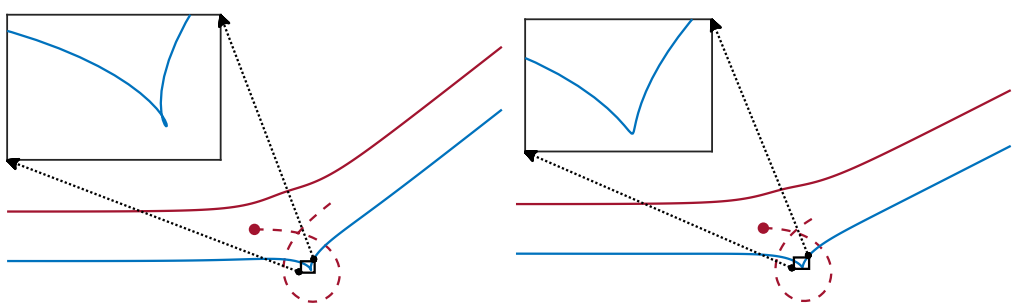

FIGURE 5.7. (Left) The vortex trajectories with $\Gamma = 0.4$ and $\rho = -0.9$. (Right) The trajectories with $\rho = -0.85$. The insets show a small loop on the trajectory of vortex 3 in the left image that has disappeared in the right image, explaining the 2π jump in the dependence of the scattering angle shown in Fig. 5.6.

6. CONCLUSION

In this paper, we have introduced a coordinate system for the three-vortex system that avoids introducing artificial singularities into the equations of motion, in contrast with previously used reduction methods. These coordinates simplify phase-space reasoning and shed new insight into the scattering between a vortex dipole and an isolated vortex.

This reduction should be useful in analyzing additional problems in point-vortex dynamics. We mention two problems we are currently considering. First, we may generalize the reduction to systems of vortices with three arbitrary circulations. Classifying how the dynamics change as the

circulations change is surprisingly complicated. A previous attempt using the triangular coordinate system is hampered by the singularity of that representation [2]. Other studies using alternative coordinate systems are entirely algebraic, focusing on relative equilibria and their stability, without the ability to visualize their organization in the global phase space [4, 10]. The approach considered here should overcome both obstacles and allow us to manage this problem's complexity better.

Second is the scattering problem in the *four-vortex* system in which two vortex dipoles collide. This problem exhibits chaotic scattering [11, 32]. Price finds a particularly simple example when the two dipoles are of widely different widths, which he calls the slingshot effect [28]. In this case, the dynamics consists of a sequence of three-vortex interactions, with the fourth vortex some distance away. The approach of this paper is one building block needed to tackle that more complex problem.

Acknowledgments

The authors gratefully acknowledge support from the NSF under DMS–2206016. We thank Emad Masroor for carefully reading this manuscript and making insightful suggestions for its improvement.

Appendix A. Calculating the scattering angle

We now calculate the change in angle $\Delta\alpha$ on trajectories with initial conditions as $t \to -\infty$ given in Fig. 2.1. The result is equivalent to one calculated in the supplementary material to Ref. [22]. We include it for completeness and to highlight the connection with the phase planes of Fig. 4.1.

To obtain an explicit integral form, we divide $\frac{\mathrm{d}\alpha}{\mathrm{d}t}$ from Eq. (3.26) by $\frac{\mathrm{d}Y}{\mathrm{d}t}$, given by Eq. (3.19b), yielding $\frac{\mathrm{d}\alpha}{\mathrm{d}Y}$. We remove the dependence on X and Z using the conservation laws (3.15) and (3.14), and then replace H by its value given the initial condition in Fig. 2.1. We will use Θ instead of ρ as the parameter in what follows because it gives somewhat simpler formulas and can use Eq. (4.5) to rewrite this in terms of the parameter ρ defining the initial conditions. Integrating this, we find

$$\Delta\alpha = \int_{Y_{\min}}^{\infty} \frac{-8\Theta^2 \mathrm{d}Y}{(Y^2+\Theta^2)\sqrt{p_4(Y^2;\Theta)}} + \int_{Y_{\min}}^{\infty} \frac{8(\Theta^2-8\Theta)\mathrm{d}Y}{(Y^2+\Theta^2-8\Theta)\sqrt{p_4(Y^2;\Theta)}} \tag{A.1}$$

where

$$p_4(Y^2;\Theta) = Y^4 + 2\left(\Theta^2 - 4\Theta - 8\right)Y^2 + (\Theta-8)\Theta^3.$$

These are *complete elliptic integrals* [7]. To place them in standard form, we must first factor $p_4(Y^2;\Theta)$. We plot its zero locus in Fig. A.1 as a function of Θ and Y^2. From this image, it is clear that p_4 can be factored as follows

$$p_4(Y^2,\Theta) = \begin{cases} (Y^2-(a+ib)^2)(Y^2-(a-ib)^2), & a>0, b>0, \text{ if } \Theta<-1; \\ (Y^2-a^2)(Y^2-b^2), & a>b>0, \text{ if } -1<\Theta<0; \\ (Y^2-a^2)(Y^2+b^2), & a>0, b>0, \text{ if } 0<\Theta<8; \\ (Y^2+a^2)(Y^2+b^2), & a>b>0, \text{ if } 8<\Theta. \end{cases} \tag{A.2}$$

The first two cases correspond to the left phase plane of Fig. 4.1, the last two to the right phase plane; the first and last cases correspond to direct scattering, and the second and third to exchange scattering. The lower limit of integration is $Y_{\min} = 0$ in the first and fourth cases, while in the second and third $Y_{\min} = a$. Both integrals in Eq. (A.1) can be evaluated with the help of references such as Gradshteyn/Ryzhik and Byrd/Friedman [7, 13]. It is quite possible that these expressions can be simplified further. For example, Lydon derived formulas in which α is the sum of one complete elliptic integral of the first kind and one of the third kind.

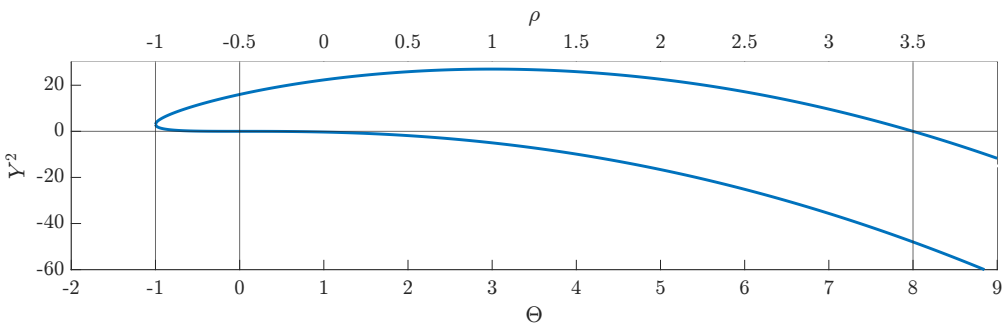

FIGURE A.1. The solutions to $p_4(Y^2, \Theta) = 0$, with the transitions between the factored form in Eq. (A.2) marked be vertical lines.

In the four regions, the constants evaluate to the following

$$a^2 = \frac{1}{2}\left(\sqrt{\Theta - 8}\Theta^{3/2} - \Theta^2 + 4\Theta + 8\right), \quad b^2 = \frac{1}{2}\left(\sqrt{\Theta - 8}\Theta^{3/2} + \Theta^2 - 4\Theta - 8\right) \qquad \text{if } \Theta < -1;$$

$$a^2 = -\Theta^2 + 4\Theta + 8\sqrt{\Theta + 1} + 8, \qquad b^2 = -\Theta^2 + 4\Theta - 8\sqrt{\Theta + 1} + 8 \qquad \text{if } -1 < \Theta < 0;$$

$$a^2 = -\Theta^2 + 4\Theta + 8\sqrt{\Theta + 1} + 8, \qquad b^2 = \Theta^2 - 4\Theta + 8\sqrt{\Theta + 1} - 8 \qquad \text{if } 0 < \Theta < 8;$$

$$a^2 = \Theta^2 - 4\Theta + 8\sqrt{\Theta + 1} - 8, \qquad b^2 = \Theta^2 - 4\Theta - 8\sqrt{\Theta + 1} - 8 \qquad \text{if } 8 < \Theta.$$

In each of the four ρ intervals, the scattering angle can be written as a linear combination of complete elliptic integrals of the first kind

$$K(m) = \int_0^1 \frac{\mathrm{d}x}{\sqrt{(1 - x^2)(1 - mx^2)}} = \int_0^{\frac{\pi}{2}} \frac{\mathrm{d}\theta}{\sqrt{1 - m\sin^2\theta}}.$$

and the third kind

$$\Pi(n, m) = \int_0^1 \frac{dx}{(1 - nx^2)\sqrt{(1 - x^2)(1 - mx^2)}} = \int_0^{\frac{\pi}{2}} \frac{\mathrm{d}\theta}{\left(1 - n\sin^2\theta\right)\sqrt{1 - m\sin^2\theta}}.$$

The convention is to define these functions for $0 < m < 1$, though they are analytic for all m except for a branch cut from $m = 1$ to $m = \infty$.

We report the values found in each of the cases.

Direct scattering with $\rho < -1$. Here $\Theta < -1$, and

$$\Delta\alpha = \frac{64\sqrt[4]{\Theta - 8}}{\sqrt[4]{\Theta}\left(\Theta - 8 + \sqrt{\Theta^2 - 8\Theta}\right)\left(\Theta + \sqrt{\Theta^2 - 8\Theta}\right)}\left(-K(m) + \Pi(n, m)\right)$$

with

$$m = \frac{1}{2} + \frac{4 - \Theta}{2\sqrt{\Theta^2 - 8\Theta}} \quad \text{and} \quad n = \frac{1}{2} - \frac{\Theta^2 - 4\Theta - 8}{2\Theta\sqrt{\Theta^2 - 8\Theta}}.$$

Exchange scattering with $-1 < \rho < -\frac{1}{2}$. In this case $-1 < \Theta < 0$, and

$$\Delta\alpha = \frac{1}{\sqrt{-\Theta^2 + 4\Theta + 8\sqrt{\Theta + 1} + 8}}\left(4\Theta K(m) + 8\sqrt{1 + \Theta}\Big(\Pi(n_1, m) - \Pi(n_2, m)\Big)\right),$$

where

$$m = \frac{8 + 4\Theta - \Theta^2 - 8\sqrt{\Theta + 1}}{8 + 4\Theta - \Theta^2 + 8\sqrt{\Theta + 1}}, n_1 = \frac{\Theta - 2 + 2\sqrt{\Theta + 1}}{\Theta + 2 - 2\sqrt{\Theta + 1}}, \quad \text{and} \quad n_2 = \frac{\Theta + 2 - 2\sqrt{\Theta + 1}}{\Theta + 2 + 2\sqrt{\Theta + 1}}.$$

The borderline case $\rho = -\frac{1}{2}$. This is the case $\Theta = 0$ discussed in Fig. 4.2. Vortex 2 travels along a straight line with no deflection, so the scattering angle is $\alpha = 0$.

Exchange scattering with $-\frac{1}{2} < \rho < \frac{7}{2}$. Here $0 < \Theta < 8$, and

$$\Delta\alpha = \frac{-\Theta^2 + 4\Theta + 8\sqrt{\Theta+1} + 8}{2\sqrt[4]{\Theta+1}\left(\Theta + 2\sqrt{\Theta+1} + 2\right)}\Big(\Pi(n_1, m) - \Pi(n_2, m)\Big),$$

where

$$m = \frac{1}{2} + \frac{\Theta^2 - 4\Theta - 8}{16\sqrt{1-\Theta}}, n_1 = \frac{2 - \Theta - 2\sqrt{1+\Theta}}{4}, \quad \text{and} \quad n_2 = \frac{2 + \Theta - 2\sqrt{1+\Theta}}{4}.$$

Direct scattering with $\frac{7}{2} < \rho$. In this last case, $\Theta > 8$ and

$$\Delta\alpha = c_K K(m) + c_{\Pi,1}\Pi_1(n_1, m) + c_{\Pi,2}\Pi(n_2, m),$$

where

$$m = \frac{16\sqrt{\Theta+1}}{\Theta^2 - 4\Theta - 8 + 8\sqrt{\Theta+1}}, n_1 = -\frac{4}{\Theta + 2\sqrt{\Theta+1} - 2}, n_2 = \frac{4\left(\Theta + 2\sqrt{\Theta+1} + 2\right)}{\Theta^2}$$

$$c_K = -\frac{4\Theta}{\sqrt{\Theta^2 - 4\Theta + 8\sqrt{\Theta+1} - 8}}, c_{\Pi,1} = \frac{-2\Theta^3 + 4\Theta^2 + 64\Theta + 64 - 4\sqrt{\Theta+1}\left(\Theta^2 - 8\Theta - 16\right)}{\sqrt{(\Theta-8)\Theta^3\left((\Theta-4)\Theta - 8\left(\sqrt{\Theta+1}+1\right)\right)}},$$

$$\text{and} \quad c_{\Pi,2} = \frac{-2\Theta^3 + 12\Theta^2 - 32\Theta - 64 + 4\left(\Theta^2 - 16\right)\sqrt{\Theta+1}}{\sqrt{(\Theta-8)\Theta^3\left((\Theta-4)\Theta - 8\left(\sqrt{\Theta+1}+1\right)\right)}}$$

References

[1] A. A. Andronov and S. E. Chaikin. *Theory of Oscillations*. United Scientific-Technical Publishing House (ONTI), Moscow, 1937. (English version 1949, Princeton University Press, Edited by S. Lefschetz and translated by N. Goldowski.).

[2] H. Aref. Motion of three vortices. *Phys. Fluids*, 22:393, 1979.

[3] H. Aref. A transformation of the point vortex equations. *Phys. Fluids*, 14:2395–2401, 2002.

[4] H. Aref. Stability of relative equilibria of three vortices. *Phys. Fluids*, 21:094101, 2009.

[5] H. Aref, N. Rott, and H. Thomann. Gröbli's solution of the three-vortex problem. *Ann. Rev. Fluid Mech*, 24:1 – 21, 1992.

[6] D. Blackmore, L. Ting, and O. Knio. Studies of perturbed three vortex dynamics. *J. Math. Phys.*, 48:065402, 2007.

[7] P. Byrd and M. Friedman. *Handbook of Elliptic Integrals for Engineers and Scientists*. Grundlehren der mathematischen Wissenschaften. Springer Berlin Heidelberg, 2nd edition, 1971.

[8] D. M. F. Chapman. Ideal vortex motion in two dimensions: Symmetries and conservation laws. *J. Math. Phys.*, 19:1988–1992, 1978.

[9] A. J. Chorin and J. E. Marsden. *A Mathematical Introduction to Fluid Mechanics*, volume 4 of *Texts in Applied Mathematics*. Springer-Verlag, 3rd edition, 1993.

[10] R. Conte and L. de Seze. Exact solution of the planar motion of three arbitrary point vortices. *Mod. Phys. Lett. B*, 29:1530017, 2015.

[11] B. Eckhardt and H. Aref. Integrable and chaotic motions of four vortices II. Collision dynamics of vortex pairs. *Philos. Trans. R. Soc. London, Ser. A*, 326:655 – 696, 1988.

[12] R. Goodman. An English Translation of Gröbli's Ph.D. Dissertation: "Specielle Probleme über die Bewegung geradliniger paralleler Wirbelfäden". submitted to arXiv.org, 2024.

[13] I. Gradshteyn and I. Ryzhik. *Table of Integrals, Series, and Products*. Elsevier Science, 2014.

[14] W. Gröbli. *Spezielle probleme Über die Bewegung geradliniger paralleler Wirbelfäden.* PhD thesis, Georg-August-Universität Göttingen, 1877.
[15] D. D. Holm. *Geometric Mechanics Part I: Dynamics and Symmetry.* Imperial College Press, 2nd edition, 2011.
[16] D. D. Holm. *Geometric Mechanics Part II: Rotating, translating and rolling.* Imperial College Press, 2nd edition, 2011.
[17] D. D. Holm, T. Schmah, and C. Stoica. *Geometric Mechanics and Symmetry.* Oxford University Press. Oxford University Press, 07 2009.
[18] C. G. J. Jacobi. *Vorlesungen über Dynamik.* C. F. Amelangsche Verlagsbuchhandlung, 1866.
[19] G. Kirchhoff. *Vorlesungen über mathematische Physik: Mechanik*, volume 1 of *Vorlesungen über mathematische Physik.* Teubner, Leipzig, 1876.
[20] V. S. Krishnamurthy, H. Aref, and M. A. Stremler. Evolving geometry of a vortex triangle. *Phys. Rev. Fluids*, 3:024702, 2018.
[21] Q. Luo, Y. Chen, and Q. Liu. Global phase diagrams of three point vortices. *Int. J. Bifurcation Chaos*, 32:2250025, 2022.
[22] K. Lydon, S. V. Nazarenko, and J. Laurie. Dipole dynamics in the point vortex model. *J. Phys. A: Math. Theor.*, 55:385702, 2022.
[23] V. V. Meleshko and H. Aref. A bibliography of vortex dynamics 1858-1956. *Adv. Appl. Mech.*, 41:197–292, 2007.
[24] A. Müller and P. Névir. A geometric application of Nambu mechanics: The motion of three point vortices in the plane. *J. Phys. A: Math. Theor.*, 47:105201 – 16, 2014.
[25] Y. Nambu. Generalized Hamiltonian dynamics. *Phys. Rev. D*, 7:2405–2412, 1973.
[26] P. K. Newton. *The N-Vortex Problem, Analytical Techniques.* Springer, 2001.
[27] E. A. Novikov. Dynamics and statistics of a system of vortices. *Soviet Physics JETP*, 41:937–943, 1975.
[28] T. Price. Chaotic scattering of two identical point vortex pairs. *Phys. Fluids A*, 5:2479–2473, 1993.
[29] S. A. Smith and B. M. Boghosian. Robust numerical method for integration of point-vortex trajectories in two dimensions. *Phys. Rev. E*, 83:056702, 2011.
[30] J. L. Synge. On the motion of three vortices. *Can. J. Math.*, 1:257–270, 1949.
[31] J. Tavantzis and L. Ting. The dynamics of three vortices revisited. *Phys. Fluids*, 31:1392, 1988.
[32] L. Tophøj and H. Aref. Chaotic scattering of two identical point vortex pairs revisited. *Phys. Fluids*, 20:093605, 2008.
[33] H. von Helmholtz. Über Integrale der hydrodynamischen Gleichungen, welcheden Wirbelbewegungen entsprechen. *J. Reine Angew. Math*, 55:25–55, 1858.